ARTICLE

3-[[3-(Triethoxysilyl)propyl]amino]propane-1-sulfonic Acid—Poly(vinyl alcohol) Cross-Linked Zwitterionic Polymer Electrolyte Membranes for Direct Methanol Fuel Cell Applications

Bijay P. Tripathi and Vinod K. Shahi*

Electro-Membrane Processes Division, Central Salt and Marine Chemicals Research Institute, Council of Scientific & Industrial Research (CSIR), G. B. Marg, Bhavnagar 364002, Gujarat, India

ABSTRACT Recently, organic—inorganic nanocomposite zwitterionic polymer electrolyte membranes (PEMs) have attracted remarkable interest for application to the direct methanol fuel cell (DMFC) operated at intermediate temperature (100—200 °C). In this paper, we report the synthesis of an organic—inorganic hybrid zwitterionomer silica precursor with ammonium and sulfonic acid functionality by the ring-opening of 3-propanesultone under mild heating conditions and the preparation procedure of a proton-conductive and stable organic—inorganic zwitterion—poly(vinyl alcohol) (PVA) cross-linked PEM by sol—gel in aqueous media. Developed PEMs were extensively characterized by studying their physicochemical and electrochemical properties under DMFC operating conditions. These membranes were designed to possess all of the required properties of a proton-conductive membrane, namely, reasonable swelling, good mechanical, dimensional, and oxidative strength, flexibility, and low methanol permeability along with reasonable proton conductivity (4.85×10^{-2} S cm^{-1}) due to zwitterionic functionality. Moreover, from the selectivity parameter among all developed membranes, ZI-70 [zwitterionomer membrane with 70 wt % of PVA of 3-[[3-(triethoxysilyl)propyl]amino]propane-1-sulfonic acid in the membrane matrix], exhibited the best results in comparison to the Nafion117 membrane for DMFC applications.

KEYWORDS: zwitterionic polymer electrolyte membrane • sol—gel • organic—inorganic composite • direct methanol fuel cell

1. INTRODUCTION

Direct methanol fuel cells (DMFCs) are being pushed toward the brink of commercialization because they offer the potential of longer operating lifetimes and the ability to refuel versus recharge compared to the batteries typically used in portable power applications (1—3). DMFC offers a reasonably high fuel energy density, a readily stored and available liquid fuel, ease of refueling, and direct and complete electrooxidation of methanol at moderate temperatures (80—120 °C) (4—6). Significant research effort has been focused on the development of new proton-conductive membranes for improved DMFC performance (7). Well-studied perfluorosulfonic acid polymer electrolyte membranes (PEMs) such as Nafion have been the reference membranes for DMFC because of their high electrochemical properties as well as excellent chemical stability (8—12). However, there is much interest in alternative PEMs because of Nafion's reduced performance above 80 °C, high methanol crossover, and cost (13, 14). Therefore, PEMs with high proton conductivity at intermediate temperatures under anhydrous or low-humidity conditions, environmental affability with low methanol crossover, and production cost have attracted much interest recently for problem solving in current technologies (12, 15—18). For the development of cheaper PEMs, fluorine-free materials with properties comparable to those of Nafion, based on sulfonated aromatic polymers, irradiation graft polymers, and cross-linked and blend polymers, were successfully proposed (19—24).

Nanostructured organic—inorganic hybrid materials have attracted much attention because they constitute a unique class of materials combining the properties of organic moieties (e.g., flexibility, dielectric, ductility, and processability) and the inorganic matrix (e.g., rigidity and thermal stability) and, additionally, they are synthesized through an easy processing route with low cost and less environmental impact (17, 21, 24—30). In the development of PEMs, several investigators reported that either functional groups were introduced on the organic part or polyelectrolytes were doped in the host matrix (9, 16, 31, 32). The problem associated with these types of composite materials was either excessive swelling of the organic part due to its functionalization or leaching of proton carriers upon prolonged use at elevated temperature (11, 25, 27, 33). Reports are available for diversified applications of zwitterion-based hybrid nanostructured materials, but fewer efforts have been rendered for applications as PEMs (28, 34—38). The acid—base composite PEMs with high proton conductivity under anhydrous conditions have been reported on materials such as poly(benzimidazole)phosphoric acid or -sulfuric acid (39, 40), a poly(vinylphosphonic acid) heterocycle (41), and ionic liquids (42). However, the proton-conductive pathway can be controlled by a suitable molecular assembly between acidic and basic moieties by introducing these functional

* Phone: +91-278-2569445. Fax: +91-278-2567562/2566970. E-mail: vkshahi@csmcri.org orvinodshahi1@yahoo.com.
Received for review December 11, 2008 and accepted April 9, 2009

DOI: 10.1021/am800228s

Published on Web 04/28/2009

Scheme 1. Preparation of an Organic–Inorganic Zwitterionomer Precursor

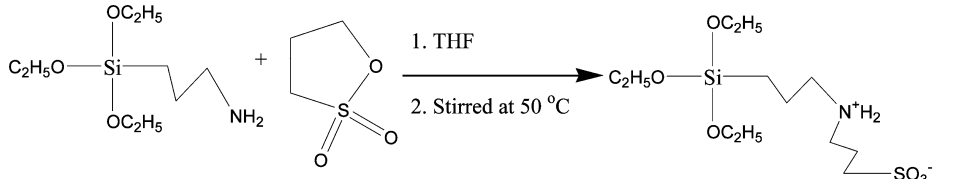

3-aminopropyltrethoxysilane 3-propanesultone (3-(3-(triethoxysilyl)propylamino)propane-1-sulfonic acid (Zwitterionomer)

groups in the same molecule for high proton conductivity, water retention, and low methanol permeability (43–45). In this manuscript, we report the synthesis procedure of a novel organic–inorganic nanocomposite zwitterionomer containing acid and base functional groups and the preparation of organic–inorganic nanocomposite zwitterionic PEMs by sol–gel.

2. EXPERIMENTAL SECTION

2.1. Materials. (3-Aminopropyl)triethoxysilane (APTEOS), tetraethoxysilane (TEOS), 3-propanesultone (distilled under vacuum), and Nafion117 (perfluorinated membrane) were purchased from Sigma Aldrich Chemicals and were used as received. Tetrahydrofuran (THF; Qualigens Fine Chemicals, Mumbai, India) was distilled and kept dry over molecular sieves. Poly(vinyl alcohol) (PVA; MW, 125 000; degree of polymerization, 1700; degree of hydrolysis, 88%), and all other chemicals, reported in this manuscript were obtained from SD Fine Chemicals (Mumbai, India) of AR grade and used without further purification. In all experiments, double-distilled water was used.

2.2. Preparation of the Zwitterionomer. The organic–inorganic precursor of the zwitterionomer, 3-[[3-(triethoxysilyl)-propyl]amino]propane-1-sulfonic acid (TPAPS), was synthesized from 3-propanesultone and APTEOS according to Scheme 1. In a general synthesis method, APTEOS in THF was stirred under a nitrogen atmosphere, 3-propanesultone dissolved in THF was added in a dropwise manner, and the reaction temperature was controlled under 60 °C, as the exothermic nature of the reaction. This reaction mixture was refluxed under stirring at 50 °C for 1 h under a nitrogen atmosphere, and the solvent was evaporated. Thus, the obtained solid mass was dried under vacuum at 40 °C for 24 h, which yields a pale-yellow-colored solid product (TPAPS).

^{1}H NMR (500 MHz, D_2O–DCl, δ): 0.8 (−SiCH_2CH_2−), 1.1 and 3.6–3.7 (−SiOC_2H_5), 1.9 (−SiCH_2CH_2−), 2.2 and 3.4 (−N$H_2^+CH_2CH_2CH_2SO_3^-$), 3.0–3.2 (−$CH_2NH_2^+CH_2$−). CHNS: calcd (C, 41.98; H, 8.45; N, 4.08; S, 9.32); obsd (C, 42.34; H, 7.95; N, 4.28; S, 10.02).

2.3. Preparation of a Cross-Linked PVA–Zwitterionomer Membrane. The membranes were prepared by a solution-casting method. A desired amount of PVA was dissolved in hot deionized water to obtain a 10 wt % solution under stirring. The appropriate amount of synthesized TPAPS was dissolved in deionized water at pH ∼ 2 and mixed with a PVA solution. A known amount of TEOS (20 wt % to PVA) was also added to cross-link the zwitterionomers to each other. Thus, the obtained solution was stirred for 6 h at room temperature. The sol–gel process was achieved by acid hydrolysis (at pH = 2) of silanes, and the hydrogen-bonded gel matrix was cast in film form on a clean poly(vinyl chloride) sheet. The film was dried in ambient conditions for 24 h and further at 70 °C for 12 h. Thus, the obtained transparent membrane was peeled off from the poly(vinyl chloride) sheet and cross-linked with a formal solution (HCHO + H_2SO_4) for 3 h at 60 °C. Prepared membranes were designated as ZI-X, where X is the weight percent of zwitterionomer (TPAPS) in the membrane matrix. The value of X varied between 30 and 70 wt % of the PVA content.

2.4. Membrane Characterization. 2.4.1. *Fourier Transform Infrared (FTIR) and NMR Spectroscopy.* FTIR spectra of dried membrane samples were recorded using an attenuated total reflectance (ATR) technique with a Spectrum GX series 49387 spectrometer in the range of 4000–600 cm^{-1}. The IR spectrum for a synthesized zwitterionomer was obtained by the KBr pellet method. ^{1}H NMR spectra were used to characterize the synthesized zwitterionic material recorded by an NMR spectrometer (Brüker, 500 MHz) in a D_2O–DCl solvent.

2.4.2. *Thermal and Mechanical Strength Analysis.* The thermal degradation processes and stabilities of the membranes were investigated using a thermogravimetric analyzer (Mettler Toledo TGA/SDTA851 with *Star* software) under a nitrogen atmosphere with a heating rate of 10 °C/min from 50 to 600 °C. Differential scanning calorimetry (DSC) measurements were carried out in a temperature range of 30–400 °C with a heating rate of 5 °C/min. The dynamic mechanical stabilities of the composite membranes were evaluated by using a Mettler Toledo dynamic mechanical analyzer 861 instrument with *Star* software under nitrogen with a heating rate of 10 °C/min from 30 to 300 °C to verify the effect of the silica content in the form of a zwitteriommer.

2.4.3. *Microscopic Characterizations.* Scanning electron microscopy (SEM) images of the dried membranes were recorded using a LEO Instruments (Kowloon, Hong Kong) microscope after gold sputter coatings on desired membrane samples. The presence of silica and other elements in the membrane was detected by energy-dispersive X-ray (EDX) measurements, carried out using a LEO VP1430 and an Oxford Instruments (Oxfordshire, U.K.) INCA.

2.4.4. *Uptake and State of Water.* The water uptake was evaluated from the difference in mass before and after the complete drying of the membranes using the following equation:

$$\text{water uptake } (\phi_w) = \frac{W_{wet} - W_{dry}}{W_{dry}} \times 100\% \qquad (1)$$

where W_{wet} and W_{dry} are the masses of the membrane under wet and dry conditions.

Freezing water (loosely bound and free water) and nonfreezing water (bound water) in the fully swelled membrane were analyzed by DSC studies using a low-temperature measuring head and a liquid-nitrogen-cooled heating element. The types of bound or loosely bound water were detected by a melting transition in DSC measurements as described elsewhere (46–51). The membrane samples were cooled from +25 to −50 °C and then heated at a rate of 2 °C/min up to +50 °C. The peak area of the melt endotherm obtained by integration was used for the estimation of bulk water. The degree of crystallinity of the water, obtained from the heat of fusion of pure ice, 333.5 J/g, was used as a standard.

2.4.5. *Membrane Water Retention Studies.* The water retention ability of the developed membranes was evaluated by measuring the water mobility during the dynamic deswelling test (52). Fully swollen membranes were placed in a thermogravimetric analyzer at 40 °C, and the loss in weight was recorded with time intervals of 12 s for 120 min. The weight of

fully swollen membranes (W_{wet}), weight of membranes at time t (W_t), and weight of dry membranes (W_{dry}) were recorded. The deswelling profile can be obtained by plotting (M_t/M_0)−time curves using the equation

$$\frac{M_t}{M_0} = 4\left(\frac{Dt}{\prod l^2}\right)^{1/2} \quad (2)$$

where M_0 is the initial amount of water in the membrane ($M_0 = W_{wet} - W_{dry}$), M_t is the amount of water remaining in the membrane at any given time ($M_t = W_t - W_{dry}$), D is the water diffusion coefficient, and l is the membrane thickness.

2.4.6. *Dimensional, Oxidative, and Hydrolytic Stabilities.* The dimensional stability was examined by immersing the square pieces of the membranes in room temperature water and 50% water−methanol for 24 h as reported previously (53). The oxidative stability was evaluated by immersing the membrane samples in Fenton's reagent (3% aqueous H_2O_2 + 3 ppm $FeSO_4$) at 80 °C for 1 h as reported previously (53). For the hydrolytic stability test, a small piece of membrane was boiled in water for 24 h at 140 °C in a pressurized closed vial. The stability was evaluated by the weight loss observed in the membrane after stability evaluation and the appearance of the test samples.

2.4.7. *Ion-Exchange Capacity (IEC).* IEC is defined as the ratio between the number of exchangeable sulfonic acid groups (equivalents) and the weight of the dry membrane. IEC by the titration method (IEC_{tit}) was determined after ion exchange of the counterion as reported previously (26, 54). Pieces of the membrane samples with known dry weight were equilibrated in 1.0 M HCl for converting all charge sites into the H^+ form. The membranes were then washed thoroughly with double-distilled water to remove the last trace of acid. Then they were equilibrated in a known volume of 1.0 M NaCl for 24 h to replace the H^+ ions with Na^+ ions. The remaining solution was titrated against a 0.1 M NaOH solution using phenolphthalein as an indicator.

IEC by the elemental analysis method (IEC_{ea}) was calculated from the sulfur content obtained by elemental analysis using the equation (8)

$$IEC_{ea} = \frac{1000S}{\text{AW of } S} \quad (3)$$

where S corresponds to the sulfur content determined by elemental analysis, the atomic weight (AW) of sulfur is 32 g/mol, and 1000 is the multiplying factor to obtain an IEC value in mmol/g.

2.4.8. *Proton Conductivity and Transport Numbers.* Membrane conductivity measurements were performed in a cell composed of two platinum electrodes, separated by the membrane with a 1 cm^2 effective area. There was provision to pass hot water of a desired temperature into each compartment, and the actual temperature was monitored at the vicinity of the membrane surface with the help of two thermocouples. The membrane conductivity in terms of membrane resistance was recorded using two potentiostatic electrode modes by an alternating current (ac), with the help of a digital conductivity meter (Century model CC601, conductance range 0−200 mS, frequency 1−50 kHz, up to ±0.001 mS reproducibility) (24). All measurements were carried out in 100% relative humidity conditions.

The proton transport number in the membrane phase was obtained by membrane potential measurements, carried out in a two-compartment cell separated by a membrane (7 cm^2). Both of the compartments were filled by HCl solutions of two different concentrations ($C_1/C_2 = 10$). For the minimum boundary layer effect, both of the compartments were vigorously stirred by magnetic stirrers. The potential difference, developed across the membrane reproducible up to 0.10 mV, was recorded using a saturated calomel electrode and salt bridges. Proton transport numbers in the membrane phase ($t_{H^+}^m$) were estimated by the TMS (Teorell, Meyer, and Sievers) approach (55).

2.4.9. *Methanol Permeability.* The methanol permeability of the composite membranes was determined in a diaphragm diffusion cell, consisting of two compartments (50 cm^3) separated by a vertical membrane with a 20 cm^2 effective area. The membrane was clamped between both compartments, which were stirred during the experiments. Before the experiment, the membranes were equilibrated in a water−methanol solution for 12 h. Initially, one compartment (A) contained 30 or 50% (v/v) methanol−water mixtures and the other (B) double-distilled water. Methanol flux arises across the membrane as a result of the concentration difference between the two compartments. The increase in the methanol concentration with time in compartment B was monitored by measuring the refractive index using a digital refractometer (Mettler Toledo RE40D refractometer). The methanol permeability (P) was finally obtained by the equation (53)

$$P = \frac{1}{A}\frac{C_B(t)}{C_A(t - t_0)}V_B l \quad (4)$$

where A is the effective membrane area, l the thickness of the membrane, $C_B(t)$ the methanol concentration in compartment B at time t, $C_A(t - t_0)$ the change in the methanol concentration in compartment A between time 0 and t, and V_B the volume of compartment B. All experiments were carried out at room temperature, and the uncertainty of the measured values was less than 2%.

2.4.10. *Electroosmotic Permeability Measurements.* Electroosmotic permeability measurements were carried out in a two-compartment cell (25 cm^3) made of acrylic glass and separated by the polyelectrolyte membrane (24.0 cm^2) (26). Both chambers were kept in a state of constant agitation by means of magnetic and mechanical stirrers. A known potential difference was imposed across the membrane with the help of a potentiostat using Ag/AgCl electrodes fixed in both chambers. The resultant volumetric flux from the anodic to cathodic chamber was measured by observing the movement of liquid in a horizontal fixed capillary tube of known radius. The current flowing through the system was also measured using a digital ammeter connected in series. Several measurements were performed to obtain reproducible values.

3. RESULTS AND DISCUSSION

3.1. Synthesis of a Zwitterionomer and Membrane Preparation. An organic−inorganic hybrid zwitterionomer silica precursor was synthesized by the ring-opening of 3-propanesultone with APTEOS under mild heating conditions according to Scheme 1. Because of the highly reactive nature of 3-propanesultone with the amine group, the reaction was exothermic and was completed without any side reaction (56). Formation of the desired zwitterionomer was confirmed by ^1H NMR and FTIR spectra, presented in Figure 1A,B. The IR spectrum exhibited the characteristic peaks of sulfonate groups at 1042 cm^{-1} and of hydrated sulfonic acid groups at 1472−1165 cm^{-1} (57, 58). This indicates that both sulfonate and sulfonic acid groups were present. A substituted quaternary ammonium group was confirmed by the presence of a peak at 1645 cm^{-1} and a broad absorbance in the region of 3033−2500 cm^{-1}. The peak due to the Si−OR group was merged with the peak of

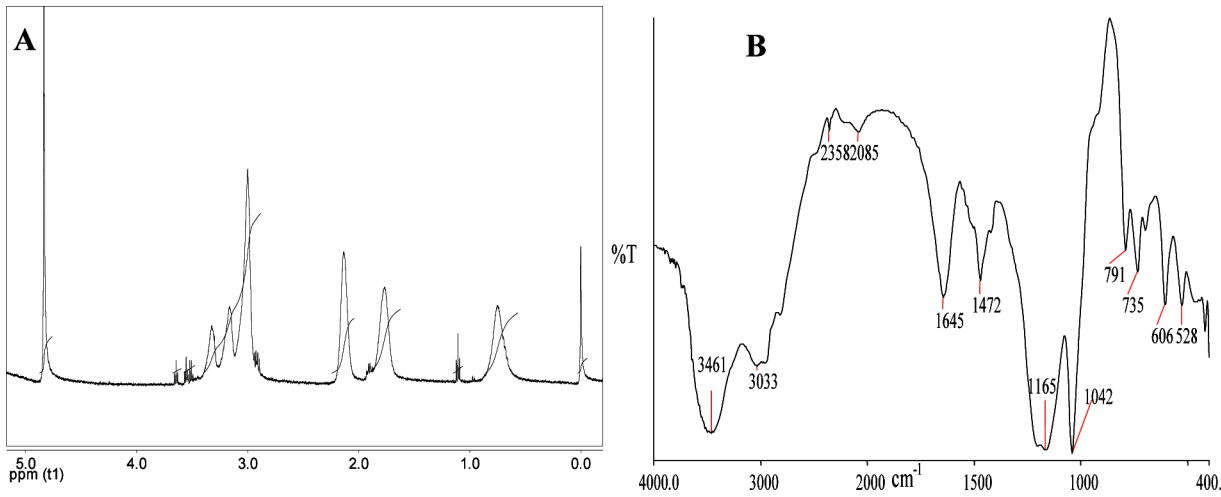

FIGURE 1. (A) ^{1}H NMR spectrum and (B) FTIR spectrum of the synthesized zwitterionic silica precursor compound 3-[[3-(triethoxysilyl)propyl]amino]propane-1-sulfonic acid.

Scheme 2. Schematic Synthetic Route of an Organic–Inorganic Zwitterionic Nanocomposite Membrane

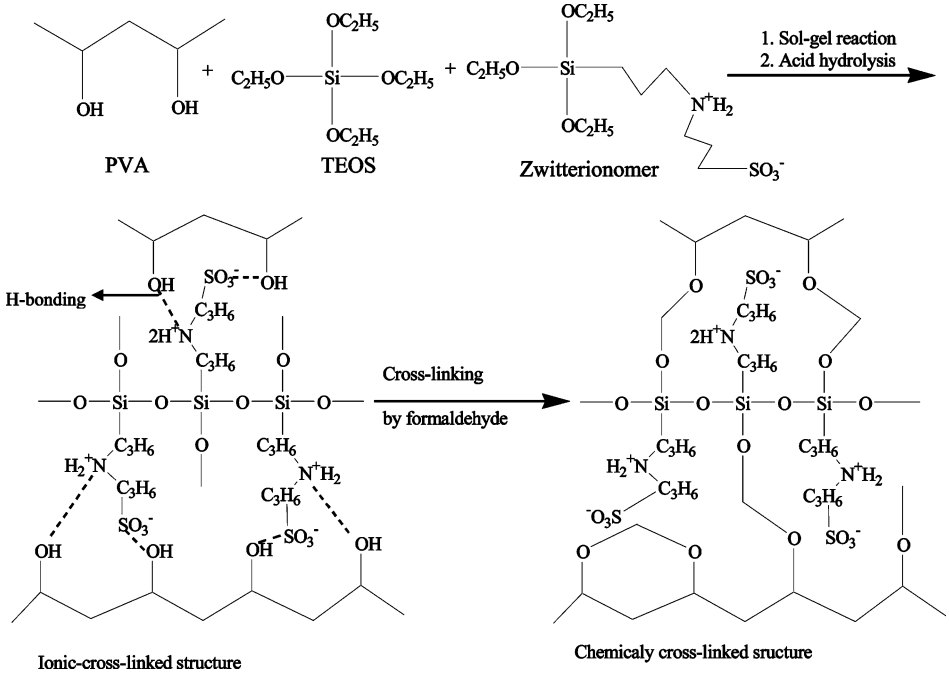

a sulfonate group and observed as a broad two-headed peak in the region of 1150–1200 cm^{-1}. The salt nature of the zwitterionomer was confirmed by the presence of two sharp peaks at 606 and 528 cm^{-1}.

Membrane-forming material was prepared by the condensation polymerization of the synthesized zwitterionic silica precursor in aqueous media using PVA by an acid-catalyzed sol–gel process according to Scheme 2. Obtained transparent water-soluble thin films were cross-linked by HCHO in the presence of acid for a constant 3 h under hot conditions. The cross-linking process with formaldehyde is a two-step process. The formaldehyde reacts with a hydroxyl group of PVA and forms hemiacetal in the first step. This hemiacetal undergoes further reaction with another hydroxyl group and results in acetal formation in the second step. Because of cross-linking, the membrane lost its transparent nature in the wet state but retained it in the dry state. The organic–inorganic composite up to the molecular level was achieved by the sol–gel method, in which both segments, inorganic and organic, were joined by covalent or hydrogen bonding.

The effect of the nature of the catalysts and its effect on membrane properties in the sol–gel process were also investigated in acidic and basic media. Both catalyzed reactions (acid and base) were bimolecular nucleophilic substitution reactions. However, the acid-catalyzed mechanisms were preceded by rapid protonation of the OR or OH substituents bonded directly to the Si atom, whereas under basic conditions, hydroxyl or silanolate anions attacked the Si atom directly. With time, sufficient numbers of interconnected Si–O–Si bonds are formed in a region; they interact cooperatively to form colloidal particles or a sol, and further colloidal particles link together to form a three-dimensional network or a gel. Acid catalysis forms linear polymers, which

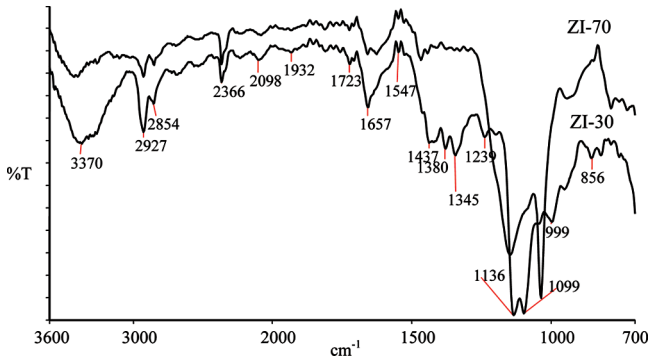

FIGURE 2. ATR FTIR spectra of ZI-30 and ZI-70 nanocomposite membranes.

are weakly cross-linked because of steric crowding, while base catalysis forms more highly branched clusters because of more rapid hydrolysis (27). Under acidic conditions (pH = 2), the obtained membrane showed good mechanical and electrochemical properties, while under basic media (base-catalyzed sol−gel process), the membrane showed deterioration of the mechanical and electrochemical properties. In the acid/base-catalyzed sol−gel process, the silica precursor and water form a one-phase solution that goes through a solution-to-gel transformation and forms a rigid two-phase system comprised of solid silica (SiO_2) and solvent-filled pores. The ATR FTIR spectra of two representative membranes (ZI-30 and ZI-70) are presented in Figure 2. The presence of a sulfonic acid group in the membrane matrix was confirmed because of the absorption bands present in the region of 1100−1039 cm^{-1} and multiheaded bands at 1450−1350 cm^{-1} (58). Peaks in the regions of 1650−1550 and 3000−2800 cm^{-1} indicated the presence of quaternary ammonium groups and peaks at 3400−3300 cm^{-1} indicated the presence of a quaternary ammonium salt (58). The strong absorption band in the region of 1150−1030 cm^{-1} aroused because of the cyclodiether part (−C−O−C−) confirmed the cross-linked structure of the membrane matrix. The intensity of these peaks varied with the zwitterionomer content in the membrane. The absorption bands in the region of 1150−1050 cm^{-1} (characteristic Si−O−Si asymmetric stretching and Si−O−C) indicated hybridization at the molecular level between organic and inorganic components. It is clear that Si−O−Si groups are the result of a condensation reaction between hydrolyzed silanol (SiOH) groups, and the Si−O−C groups may originate from the condensation reaction between the SiOH group from a hydrolyzed zwitterionomer and TEOS and COH groups from PVA. In acidic conditions, PVA could react with the cross-linking agent and silanol groups and may result in the C−O−C (1300−1200 cm^{-1}) and Si−O−C groups. The formation of Si−O−C and C−O−C groups will be in favor of better compatibility between organic and inorganic components, and a better homogeneity of the inorganic and organic matrix at the molecular scale leads to a highly thermal and mechanical stable membrane.

3.2. Thermal and Mechanical Stability. The thermal degradation property of ZI-X membranes in the H^+ form was assessed by thermogravimetric analysis (TGA) as presented in Figure S1 in the Supporting Information. The nanocomposite films exhibited a three-step weight loss pattern. The first weight loss at 30−130 °C (8−10% of the initial weight) was considered to be due to the evaporation of residual water present in the membrane matrix and water produced as a result of further condensation between the hydroxyl groups of a zwitterionomer and PVA (46). In this region, the ZI-30 membrane showed the lowest weight loss in comparison to the membranes with a higher weight percentage of zwitterionomer, maybe because of the lower amount of water present in the matrix. The second weight loss (15−20% of the initial weight) occurred in the region of 150−250 °C, which was attributed to the decomposition of sulfonic acid groups (SO_2 and SO_3) and the cleavage of the PVA chain (46). In this step, the ZI-30 membrane showed lower weight loss character, while the ZI-50 and ZI-70 membranes showed slightly higher and early weight loss. This observation was attributed to the higher cross-linked structure of the PVA chain and the lower sulfonic acid content in ZI-30. The membranes further deteriorated beyond 300 °C and showed a steep weight loss pattern.

DSC analysis was carried out in a nitrogen atmosphere with a 5 °C/min heating rate, and results for the ZI-30, ZI-50, and ZI-70 membranes are presented in Figure S2 in the Supporting Information. The first endothermic peaks corresponding to the T_g values was found to be around 107.5, 105.2, and 102.5 °C, respectively. The second endothermic peaks were obtained at temperatures of 185.8, 209.1, and 214.1 °C for ZI-30, ZI-50, and ZI-70 membranes, respectively. The incorporation of a zwitterionomer in PVA had a profound effect on its T_g value. The first T_g value was found to decrease with an increase in the zwitterionomer content, maybe because of the loss of an ordered arrangement of the organic−inorganic component. The second T_g value increased with the zwitterionomer content, maybe because of an enhanced cross-linked structure at higher temperature. T_g of pristine PVA was found to be 78 °C (46, 59). These results, in combination with TGA studies, indicate that ZI-X membranes are considered to be thermally stable at moderate temperatures (100−150 °C) in a dry nitrogen atmosphere.

Figure S3 in the Supporting Information shows the effect of the zwitterionomer content on the dynamic mechanical properties of nanocomposite membranes, which showed elongation with temperature. Also, elongation increased with the zwitteionomer content. It was observed that the Zi-50 membrane showed the highest stress tolerance. This variation may be attributed to the more cross-linked nature of the ZI-50 membrane, while a further increase in the inorganic content in the membrane matrix leads to the formation of agglomerates and thus results in a loss in mechanical behavior. In PVA, the hydroxyl groups contributed to the stiffness of the linear polymeric membrane by hydrogen bonding. With a reduction in the number of hydroxyl group either by branching or cross-linking, the hydrogen bonding was reduced and thus the chain stiffness decreased. Furthermore, SiOH groups undergo inter- and intramolecular cross-linking with PVA and silica. Intermolecular cross-

Table 1. Water Uptake (φ_w), Water−Methanol Uptake (φ_{w+MeOH}), Number of Water Molecules per Ionic Site (λ_w), Volume Expansion in a Water−Methanol Solution (ϕ_v), Oxidative and Hydrolytic Weight Loss (W_{OX} and W_{HS}, Respectively), and Water Diffusion Coefficient (D) Values for Different ZI-X Membranes

membrane	φ_w (wt %)	φ_{w+MeOH} (wt %)	λ_w/SO_3^-	ϕ_v (vol %)	W_{OX} (wt %)	W_{HS} (wt %)	$D/10^{-6}$ (cm^2/s)
ZI-30	34.8	36.7	31.0	37.0	7.09	8.65	3.19
ZI-50	38.1	42.9	23.3	37.9	8.0	9.24	1.38
ZI-70	45.3	45.3	17.0	47.6	10.48	10.97	1.29

linking largely takes place at low inorganic concentration and intramolecular cross-linking at high concentration and thus produce agglomerates of the zwitterionomer. These membranes did not show any breakage up to a temperature of 250 °C.

3.3. Oxidative and Hydrolytic Stabilities. Membrane stability and durability are the most desired requirements for PEMs. The formation of H_2O_2, •OH, and •OOH radicals during water decomposition is believed to attack hydrogen-containing bonds in PEMs. Fenton's reagent (3% aqueous H_2O_2 + 3 ppm $FeSO_4$) was used to assess the stability of membranes toward oxidative conditions, and the result is included as an oxidative weight loss percent (W_{OX}) in Table 1. W_{OX} increased with the zwitterionomer content in the membrane matrix, maybe because free-radical attack is more aggressive at higher temperatures (80 °C) and occurs in the proximity of hydrophilic domains (60). The ZI-70 membrane contained more hydrophilic functionality and hydrogen-containing groups, thus exhibiting higher weight loss. The methylene moieties present in the PVA chain are very sensitive toward free-radical attacks. The radical attack produces a free radical on the PVA chain, which may be further attacked by radicals, and thus chain degradation takes place. Thus, Fenton's exposure to the long-chain PVA causes it to break into short chains. Silica blocks the hydrogen-containing hydrophilic pores by forming a cross-linked structure. The lifetime of •OH or •OOH radicals is very short (61); thus, they cannot penetrate inside the siloxane-containing domains.

Nanocomposite membranes were also subjected to accelerated hydrolytic stability testing at 140 °C and 100% relative humidity for 24 h. All of the membranes retained their transparency, flexibility, and toughness. It was observed that these membranes were less stable in hydrolytic conditions and showed a higher weight loss (W_{HS}) in comparison to the results of oxidative conditions (Table 1).

3.4. Surface Morphology and EDX Studies. SEM images of ZI-30, ZI-50, and ZI-70 membranes are presented in Figure S4A−C in the Supporting Information. Polycondensation of the zwitterionomer led to conglomeration in the membrane matrix, which increased with the silica content. Polycondensation reaction between zwitterionomers formed silica particles dispersed in the PVA matrix, because of an excessive amount of zwitterionomer. Thus, relatively larger quaternary ammonium and propylsulfonic acid groups exhibited a size exclusive effect and resulted in a grater distance between PVA chains. Further, the absence of cracks and holes in the membrane suggested their homogeneous and dense nature. The SEM-EDX spectrum of the representative ZI-50 membrane (Figure S4D in the Supporting Information) clearly indicated the presence of inorganic and organic constituents in the membrane matrix. The existence of Si, S, and N indicates that the zwitterionomer was stable in the membrane matrix. Membrane preparation by the sol−gel method is more advantageous in obtaining a membrane with a uniform and homogeneously distributed inorganic-in-organic polymer matrix. These results suggest a uniform hybrid membrane with nanosized silica and sulfonic acid clusters in the membrane phase.

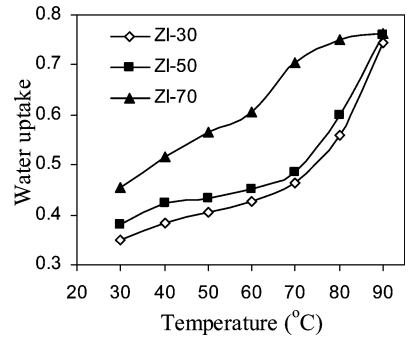

FIGURE 3. Effect of the temperature on the water uptake for different ZI-X nanocomposite membranes.

3.5. Solvent Uptake, Dimensional Changes, and Water Retention Capability. A high water content in the membrane phase leads to deterioration in the thermal, mechanical, and chemical stabilities and H^+ concentration. Water uptake (φ_w) values of the ZI-X membranes increased with the zwitterionomer content (Table 1), maybe because of the enhanced hydrophilic nature of the membrane matrix. The solvent uptake was also studied in a water−methanol mixture to assess their suitability in DMFCs, and the data are included in the same table. It was observed that these membranes showed slightly higher water−methanol uptake compared with the water uptake. The water uptake characteristics for all membranes were also measured at different temperatures, and the data are presented in Figure 3. ZI-30 and ZI-50 membranes initially showed slow increases in the water uptake up to 70 °C, while the ZI-70 membrane showed a linear increase. Beyond 70 °C, φ_w values increased steeply for the former two membranes and gently for the latter membrane. At lower temperature, the hydrophilic nature controlled the water uptake, while at higher temperature, the enhanced swelling created more space for water in the membrane matrix. In the case of the ZI-70 membrane, because of the high zwitterionomer content, more hydrophilic groups were available for hydrogen bonding with water. Also, a further increase in the inorganic content limits an increase in the dimension of the hydrophilic domains due to enhanced siloxane formation.

The total number of water molecules per ionic site (λ_w) and volume expansion (ϕ_v) values for different membranes are also presented in Table 1, as their swelling properties. The same trends of ϕ_v and φ_w values support the formation

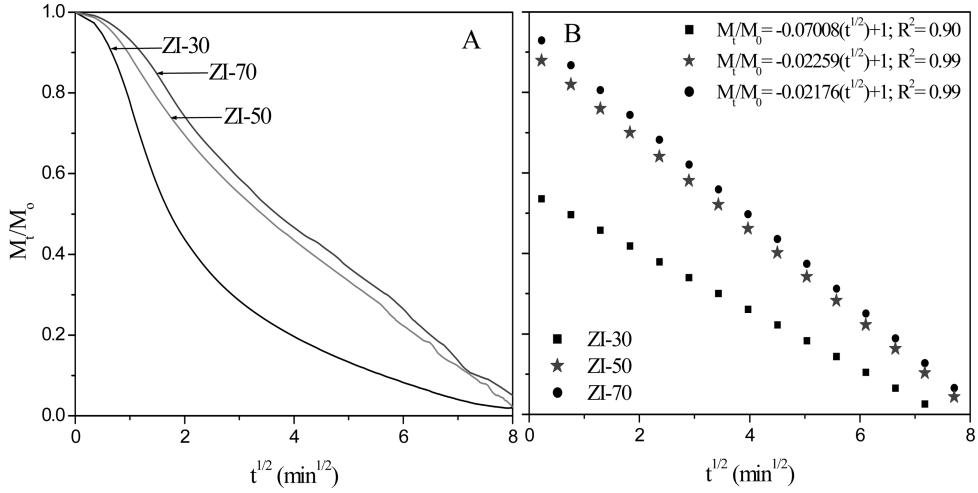

FIGURE 4. Water desorption profile for ZI-X membranes: (A) isotherm at 40 °C; (B) Higuchi's model fit of the deswelling behavior.

of a highly cross-linked and rigid structure with higher zwitterionomer content.

Water vapor sorption and diffusion properties of PEMs have significant effects on the proton conductivity and thus their applicability for fuel cells. The water retention capability of developed membranes is illustrated in Figure 4A by (M_t/M_0)−t (time) curves. The deswelling kinetics of the developed membranes was further characterized by plotting (M_t/M_0−$t^{1/2}$) curves (Figure 4B) using eq 5, derived from Higuchi's model (52).

$$\frac{M_t}{M_0} = -kt^{1/2} + 1 \qquad (5)$$

where M_0 and M_t are the initial amount of water and the water remaining in the polymer matrix at any given time and k is a constant.

Straight lines were obtained upon variation of the zwitterionomer content fitted to Higuchi's model and suggested that water desorption followed a diffusion-controlled mechanism. The rate of water desorption was reduced with an increase in the zwitterionomer content. Thus, the zwitterionomer acted as water binder in the membrane matrix because of the formation of hydrophilic ionic channels and siloxane cages. The free water in the ionic membrane matrix (−N^+H_2− and −SO_3^- groups) is less mobile and indicated that water was more bound in the hydrophilic domains and less apt for its dehydration. The water diffusion coefficient (D) was evaluated from a best-fit normalized mass change (Table 1) and was found to be decrease significantly with the zwitterionomer content in the membrane matrix. Thus, the zwitterionomer acted as a barrier for water release and improved the water retention capacity even at higher temperatures.

3.6. State of Water. Low-temperature DSC studies and water uptake values were used to quantify and elucidate the different types of water in the polymeric membranes. The water present in the membrane phase may be classified into three types: (i) free water (with the same temperature and enthalpy of melting as bulk water); (ii) freezing bound water (weakly bound with polar or ionic groups and shows

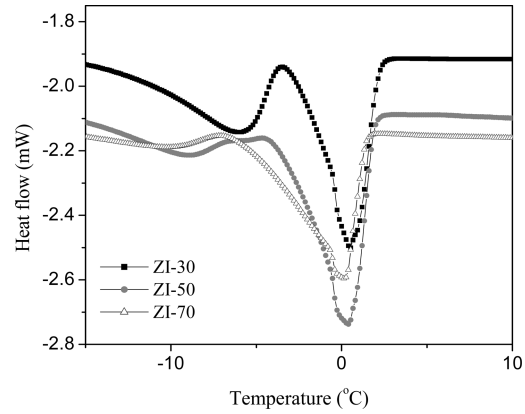

FIGURE 5. DSC melting curve for the state of water in the membrane matrix.

changes in the temperature and enthalpy compared with bulk water); (iii) nonfreezing bound water (very strong interaction with polar or ionic groups and shows no phase transition).

The DSC thermograms for hydrated ZI-X membranes (Figure 5) showed a broad endothermic peak. The melting temperature (T_m), total water content (φ_t), freezing water (φ_f), bound water (φ_b), and bound water degree (χ) for all composite membranes, determined by DSC curves, are presented in Table S1 (Supporting Information) compared with the N117 membrane (46). Comparatively higher T_m values for composite membranes may be attributed to low freezing water and high bound water percentages, which increased with the zwitterionic content in the membrane matrix.

The free water for the wet membrane was obtained from the total melting enthalpy by integration of the peak area of the melting curves (Figure 5), whereas the bound water percentage was obtained from subtraction of the freezing water content from the total water present in the membrane matrix. The degree of bound water in percentage ($\chi = \varphi_b/\varphi_f$) was estimated from the ratio of bound water to the total water. The state of free and bound water was increased with the zwitterionic content because of the increased availability of ionic sites for binding. In spite of the strong interaction

Table 2. IEC by Titration and Elemental Analysis Methods (IEC_{tit} and IEC_{ea}, Respectively), Transport Number ($t_{H^+}^m$), and Surface Charge Concentration ($C_{SO_3^-}$) Values for Different Membranes

membrane	IEC_{tit} (mequiv g^{-1})	IEC_{ea} (mmol g^{-1})	$t_{H^+}^m$	$C_{SO_3^-}/10^{-3}$ (mmol cm^{-3})
ZI-30	0.623	0.765	0.975	7.39
ZI-50	0.906	0.995	0.982	6.18
ZI-70	1.475	1.571	0.984	4.96
N117	0.91	1.0	0.938	1.10

between the ionic groups and water molecules, there are enough binding sites in the membrane to constrain water in the polymer and siloxane network and thus result in a high bound water content. The bound water degree of ZI-X membranes was optimal in comparison to that of the N117 membrane.

3.7. IEC, Transport Number, and Fixed Charge Concentration. IEC indicates the density of ionizable functional groups responsible for the proton conduction. For this membrane, the acid group interacts with two bases: its own amine and the other titrating solution of NaOH. However, the NaOH group is a very strong base and converts all $-SO_3H/SO_3^-$ groups to $-SO_3Na$ groups. This $-SO_3Na$ was changed to $-SO_3H$ by further use of a HCl solution. The possible acid–base equilibrium may be presented as follows:

$$-NH - SO_3H \xleftrightarrow{\text{ionization}} - NH_2^+ - SO_3^- \xrightarrow{\text{NaOH}}$$

$$- NH_2^+OH^- - SO_3^-Na^+ \xrightarrow{\text{HCl}} - NH_2^+Cl^- -$$

$$SO_3H \xrightarrow{\text{NaCl}}$$

$$- NH_2^+Cl^- - SO_3Na^+ + HCl$$

Thus, the produced HCl can be titrated and gives the IEC value. IECs for the zwitterionic nanocomposite and N117 membranes estimated by the titration (IEC_{tit}; mequiv g^{-1}) and elemental analysis (IEC_{ea}; mmol g^{-1}) method are presented in Table 2. IEC_{ea}, which provides the total number of sulfonic acid sites in the membrane matrix, was higher than IEC_{tit} maybe because of only accessible acidic groups estimated by the titration method. Furthermore, IEC_{ea} and IEC_{tit} both increased with the zwitterionic content in the membrane matrix and are in good agreement. Nanocomposite membranes showed higher IEC values compared with the N117 membrane.

Examination of transport numbers for H^+_{aq} in the membrane phase ($t_{H^+}^m$; Table 2) revealed that ZI-X membranes exhibited slightly higher $t_{H^+}^m$ compared with the N117 membrane, which further increased with the concentration of the zwitterionmer in the membrane matrix. Fixed surface charge concentration ($C_{SO_3^-}$) values (Table 2) were obtained from water uptake and IEC values using the equation (62)

$$C_{SO_3^-} = \frac{\text{IEC} \times \text{density of water}}{\text{water uptake (\%)}} X_V \times 100 \qquad (6)$$

where X_V is the volume function of water in a swollen membrane, estimated by the volume of water in the membrane phase. $C_{SO_3^-}$ values decreased with an increase in the zwitterionomer content in the membrane matrix because of an increase in the water uptake.

3.8. Proton Conductivity of Zwitterionic Membranes. The proton conductivity of organic–inorganic hybrid PEMs was measured at 30 °C under 100% relative humidity for hydrated membranes, and relevant data are presented in Table 3. Proton conductivity was highly dependent on the zwitterionomer content in the membrane matrix. With the zwitterionomer content in the membrane matrix, enhanced φ_w and ϕ_v values affected hydrogen bonding and thus proton conductivity, may be because of an increase in the charge careers (H_3O^+). These results support the fact that the zwitterionic sites enhanced the hydrophilic nature of the membrane and promoted water dissociation to provide protons ($2H_2O = H_3O^+ + OH^-$).

Figure 6 shows the effect of the water content on the proton conductivity of the nanocomposite zwitterionic membranes. κ^m values increased linearly with an increase in the water content in the membrane may be because water acts as an active site for proton conduction via hydrogen bonding. κ^m values increased rapidly for ZI-30 and ZI-50, while it was almost continuous for the ZI-70 membrane. After a certain value of the water content, the increase in conductivity was slowed down, which may be due to the dilution of the proton concentration, and resistance arose in the path. These variations in the proton conductivity may be rationalized by water uptake along with an increase in the free volume of the membrane.

The acidity of the synthesized TPAPS material was obtained in terms of the pK_a value, dissociation constant, and degree of dissociation. The method adopted and the titration curve are shown in Figure S5 (Supporting Information). The pK_a, dissociation constant, and degree of dissociation for TPAPS were found to 2.35, 4.5×10^{-3}, and 0.40, respectively. This indicates that all sulfonic acid groups were not dissociated in the TPAPS molecule.

The proton conductivity of the PEMs is highly dependent on the proton mobility and fixed charge concentration in the membrane matrix. Proton conductivity data were used with the advantage for estimation of the mobility of the proton (μ_{H^+}) by eq 7 (62):

$$\mu_{H^+} = \frac{\kappa^m}{FC_{SO_3^-}} \qquad (7)$$

where F is the Faraday constant. The calculated mobility of the proton in the membrane matrix ranges from 0.47×10^{-4} to 1.01×10^{-4} $cm^2\ s^{-1}\ V^{-1}$ (Table 3). The proton conductivity increased with the proton mobility because of enhanced hydration and free water volumes in the proton-conducting channels and clusters of the membrane matrix. μ_{H^+} values were dependent on IEC and φ_w values and increased with the zwitterionomer content. A higher value of the free water content assists proton conduction by reducing the tortuous path and resistance for the proton within the membrane matrix. Under similar conditions, the μ_{H^+} value for the N117 membrane was found to be 0.87×10^{-4} $cm^2\ s^{-1}\ V^{-1}$,

Table 3. Electrochemical Properties: Proton Conductivity (κ^m), Ionic Mobility (μ_{H^+}), Methanol Permeability (P), Electroosmotic Permeability (J_E), Activation Energy (E_a), and Selectivity Parameter (SP) Values for Different Membranes

membrane	$\kappa^m/10^{-2}$ (S cm^{-1})	$\mu_{H^+}/10^{-4}$ (cm^2 s^{-1} V^{-1})	$P/10^{-7}$ (cm s^{-1})	$J_E/10^{-6}$ (cm s^{-1} A^{-1})	E_a (kJ mol^{-1})	SP/10^5 (S cm^{-3} s)
ZI-30	3.42	0.47	1.14	0.89	2.69	3.00
ZI-50	4.06	0.68	3.52	1.01	3.42	1.15
ZI-70	4.85	1.01	3.95	1.14	3.13	1.23
N117	9.56	0.87	13.10	1.40	6.52	0.72

indicating a relatively easy proton conduction process compared with that of nanocomposite membranes.

Proton conductivity data obtained at elevated temperatures under 100% relative humidity are presented in Figure 7 as an Arrhenius plot for estimation of the activation energy (E_a) required for proton transport across the membrane by the equation

$$\ln \kappa^m = -\frac{E_a}{RT} \tag{8}$$

where R is the universal gas constant (8.314 J mol^{-1} K^{-1}) and T is the absolute temperature (K). All membranes exhibited positive temperature−conductivity dependencies, which suggested a thermally activated conduction process under an experimental temperature range (30−80 °C). The E_a values increased with the zwitterionomer content in the membrane matrix and ranged between 2.69 and 3.13 kJ mol^{-1} (Table 3). For nanocomposite membranes, E_a values were lower compared with the N117 membrane (6.52 kJ mol^{-1}). At higher temperature, fast proton and water molecule diffusion resulted in a rapid conduction process, due to a more continuous pathway because of interlinking hydrophilic channels. Furthermore, comparable E_a values of nanocomposite and N117 membranes indicated a Grotthus-type conduction mechanism and the usefulness of prepared membranes for DMFC applications.

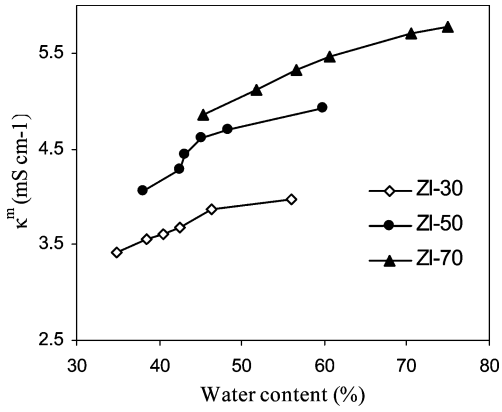

FIGURE 6. Variation of the proton conductivity with the water content for different ZI-X nanocomposite membranes.

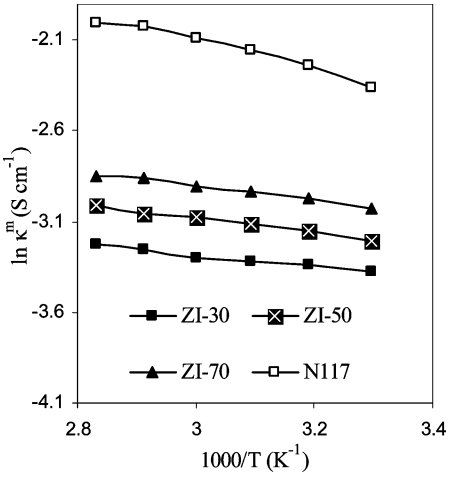

FIGURE 7. Regression curves of proton conductivity versus T^{-1} (Arrhenius plot) in a 100% relative humidity environment, for different nanocomposite and N117 membranes.

3.9. Electroosmotic Permeability Studies. A key performance limiting factor in the operation of a DMFC is the electrotransport of methanol and water through the PEM from anode to cathode. Therefore, study on the electroosmotic transport of mass (solvent) through the PEM is also essential for a better understanding of its performance. Additionally, knowledge of the electrotransport process is necessary for the intelligent design of the desired PEM (63, 64). The proton flux through the PEM leads to a water and methanol transport. In DMFCs, water and methanol transport through the PEM occurs as a result of electroosmosis (65). Electroosmotic fluxes (J_E) for different nanocomposite membranes are measured and depicted in Table 3. The electroosmotic flux was highly dependent on the zwitterionomer content in the membrane matrix. The J_E values for nanocomposite membranes were lower [$(0.89-1.14) \times 10^{-6}$ cm s^{-1} A^{-1}] in comparison with that of the N117 membrane (1.40×10^{-6} cm s^{-1} A^{-1}). Incorporation of the zwitterionomer in the membrane matrix leads to an increase in the charge carrier and also an increase in the pore volume (as observed by water uptake studies), which in turn was responsible for the higher electroosmotic flux. Thus, a definite compromise between the zwitterionomer and membrane properties is essential in order to achieve an efficient polyelectrolyte membrane.

3.10. Methanol Permeability and Selectivity Parameter Values. The methanol permeabilities through the PEMs were determined using eq 4, and the results obtained are presented in Table 3. Prepared membranes showed extremely low methanol transmission [$(1.14-3.95) \times 10^{-7}$ cm^2 s^{-1}] compared with the N117 membrane (13.10×10^{-7} cm^2 s^{-1}). The mass-transport behavior of a hydrated membrane depends on its degree of swelling, water uptake, and bulk microstructure. Methanol permeability values increased with μ_{H^+} values. It is well-known that incorporating silica particles into polymer membranes can dramatically alter their transport properties because of alteration in the free void volume and ionic clusters (17). Thus, understanding the relationship between the polymer structure and membrane

performance, in terms of permeability and selectivity, enables tailoring of the membrane structure for specific purposes. Permeation of liquid/gas molecules through the polymer membrane occurs via the diffusion mechanism, and the permeability of the penetrant (methanol) is the product of its solubility and diffusivity. The penetrant diffusivity is dependent on the free void volume in the membrane, the size of the penetrant molecules, and the segmental mobility of the polymer chain.

To directly compare the applicability of nanocomposite PEMs for DMFC applications, the ratio of the proton conductivity and methanol permeability (κ^m/P) data was used as the selectivity parameter (SP). SP values for nanocomposite and N117 membranes are also presented in Table 3. The ZI-30 membrane exhibited the highest SP value (3.00×10^5 S cm^{-3} s) among the prepared membranes. The SP value decreased with an increase in the zwitterionomer content in the membrane matrix. In similar conditions, the N117 membrane showed an SP value of 0.72×10^5 S cm^{-3} s. It was noticed that, with an increase in the operating temperature, SP values for nanocomposite membranes were also increased (Figure S6 in the Supporting Information). This observation may be attributed to the relatively low methanol permeability of the prepared membranes despite their low conductivity. These results can be explained on the basis of the lack of significant interactions between methanol and functional groups. Ionized groups hydrate strongly and excluded organic solvents (salting-out effect), which is an essential feature of the polyelectrolyte membranes. Furthermore, higher SP values of these membranes indicate a great advantage for DMFC applications.

4. CONCLUSIONS

We reported an easy synthesis of organic−inorganic hybrid zwitterionomer 3-[[3-(triethoxysilyl)propyl]amino]-propane-1-sulfonic acid, and nanocomposite PEMs were prepared by the sol−gel process in aqueous media. Monomer and membrane structure were confirmed by different spectroscopic techniques, and a schematic structure is also presented. The membrane morphology was characterized by SEM, and its composition was assessed by EDX and elemental analysis. Physicochemical and electrochemical properties of these membranes were dependent on the zwitterionomer content in the membrane matrix. Developed membranes showed good stability, flexibility, water uptake, and retention capacity. It was observed that the zwitterionomer content in the membrane matrix improved the thermal stability of ZI-X membranes, and these were thermally stable up to 200 °C in a dry nitrogen atmosphere. Among the developed membranes, ZI-70 exhibited a higher IEC value (1.475 mequiv g^{-1}), water uptake (45.32%), and proton conductivity (4.85×10^{-2} S cm^{-1}).

While these conductivity levels are not yet to the level needed for fuel cell applications, the data represent a promising starting point for the creation of more highly conducting acid−base composite systems. Furthermore, relatively lower methanol permeability and SP values of these membranes make them applicable for DMFC. The acid−base composite material may have potential applications not only for the DMFC operated at intermediate temperatures under anhydrous (water-free) or extremely low humidity conditions but also for novel electrochemical devices, where water activity is not required.

Acknowledgment. Financial assistance received from Department of Science and Technology, New Delhi (Government of India), through sponsorship of Project SR/S1/PC/06/2008 is gratefully acknowledged. Instrumental support received from Analytical Science Division, CSMCRI, is also gratefully acknowledged.

Supporting Information Available: Data of the state of water, TGA, DSC, and dynamic mechanical analysis curves, SEM images, methods for the determination of pK_a values, dissociation constants, and degree of dissociation measurements, acid−base titration curve, and selectivity parameter values of developed membranes. This material is available free of charge via the Internet at http://pubs.acs.org.

REFERENCES AND NOTES

(1) Li, Q.; He, R.; Jensen, J. O.; Bjerrum, N. J. *Chem. Mater.* **2003**, *15*, 4896.
(2) Savadogo, O. *J. Power Sources* **2004**, *127*, 135.
(3) Roziere, J.; Jones, D. J. *Annu. Rev. Mater. Res.* **2003**, *33*, 503.
(4) Alberti, G.; Casciola, M. *Annu. Rev. Mater. Res.* **2003**, *33*, 129.
(5) Jones, D. J.; Roziere, J. *Adv. Polym. Sci.* **2008**, *219*, 5219.
(6) Einsla, B. R.; Kim, Y. S.; Hickner, M. A.; Hong, Y. T.; Hill, M. L.; Pivovar, B. S.; McGrath, J. E. *J. Membr. Sci.* **2005**, *255*, 141.
(7) Colomban, P. *Proton Conductors*; Cambridge University Press: Cambridge, U.K., 1992.
(8) Pereira, F.; Valle, K.; Belleville, P.; Morin, A.; Lambert, S.; Sanchez, C. *Chem. Mater.* **2008**, *20*, 1710.
(9) Kerres, J. A. *J. Membr. Sci.* **2001**, *185*, 3.
(10) Kim, J. Y.; Choi, W. C.; Woo, S. I.; Hong, W. H. *J. Membr. Sci.* **2004**, *238*, 213.
(11) Khiterer, M.; Loy, D. A.; Cornelius, C. J.; Fujimoto, C. H.; Small, J. H.; McIntire, T. M.; Shea, K. *J. Chem. Mater.* **2006**, *18*, 3665.
(12) Costamagna, P.; Srinivasan, S. *J. Power Sources* **2001**, *102*, 242.
(13) Sone, Y.; Ekdunge, P.; Simonsson, D. *J. Electrochem. Soc.* **1996**, *143*, 1254.
(14) Sumner, J. J.; Creager, S. E.; Ma, J. J.; Desmarteau, D. D. *J. Electrochem. Soc.* **1998**, *145*, 107.
(15) Hickner, M. A.; Ghassemi, H.; Kim, Y. S.; Einsla, B. R.; McGrath, J. E. *Chem. Rev.* **2004**, *104*, 4587.
(16) Kang, M. S.; Kim, J. H.; Won, J.; Moon, S. H.; Kang, Y. S. *J. Membr. Sci.* **2005**, *147*, 127.
(17) Ladewig, B. P.; Knott, R. B.; Hill, A. J.; Riches, J. D.; White, J. W.; Martin, D. J.; Diniz da costa, J. C.; Lu, G. Q. *Chem. Mater.* **2007**, *19*, 2372.
(18) Ravikumar, M. K.; Shukla, A. K. *J. Electrochem. Soc.* **1996**, *143*, 2601.
(19) Ghassemi, H.; Ndip, G.; McGrath, J. E. *Polymer* **2004**, *45*, 5855.
(20) Zhang, X.; Liu, S.; Liu, L.; Yin, J. *Polymer* **2005**, *46*, 1719.
(21) Shahi, V. K. *Solid State Ionics* **2007**, *177*, 3395.
(22) Xing, P.; Robertson, G. P.; Guiver, M. D.; Mikhailenko, S. D.; Kaliaguine, S. *Macromolecules* **2004**, *37*, 7960.
(23) Depre, L.; Ingram, M.; Poinsignon, C.; Popall, M. *Electrochim. Acta* **2000**, *45*, 1377.
(24) Tripathi, B. P.; Shahi, V. K. *J. Colloid Interface Sci.* **2007**, *316*, 612.
(25) Binsu, V. V.; Nagarale, R. K.; Shahi, V. K. *J. Mater. Chem.* **2005**, *15*, 4823.
(26) Saxena, A.; Tripathi, B. P.; Shahi, V. K. *J. Phys. Chem. B* **2007**, *111*, 12454.
(27) Nagarale, R. K.; Gohil, G. S.; Shahi, V. K.; Rangarajan, R. *Macromolecules* **2004**, *37*, 10023.
(28) Zou, H.; Wu, S.; Shen, J. *Chem. Rev.* **2008**, *108*, 3893.

(29) Besson, E.; Mehdi, A.; Chollet, H.; Reye, C.; Guilard, R.; Corriu, R. J. P. *J. Mater. Chem.* **2008**, *18*, 1193.
(30) Xu, T. *J. Membr. Sci.* **2005**, *263*, 1.
(31) Kim, D. S.; Park, H. B.; Rhim, J. W.; Lee, Y. M. *J. Membr. Sci.* **2004**, *240*, 37.
(32) Smitha, B.; Sridhar, S.; Khan, A. A. *Macromolecules* **2004**, *37*, 2233.
(33) Wu, C.; Xu, T.; Yang, W. *J. Membr. Sci.* **2003**, *224*, 117.
(34) Liu, J.; Xu, T.; Fu, Y. *J. Membr. Sci.* **2005**, *252*, 165.
(35) Liu, J.; Xu, T.; Gong, M.; Fu, Y. *J. Membr. Sci.* **2005**, *260*, 26.
(36) Narita, A.; Shibayama, W.; Sakamoto, K.; Mizumo, T.; Matsumi, N.; Ohno, H. *Chem. Commun.* **2006**, 1926.
(37) Kim, H. S.; Park, S. J.; Nguyen, D. Q.; Bae, J. Y.; Bae, H. W.; Lee, H.; Lee, S. D.; Choi, D. K. *Green Chem.* **2007**, *9*, 599.
(38) Innocenzi, P.; Brusatin, G. *Chem. Mater.* **2000**, *12*, 3726.
(39) Schechter, A.; Savinell, R. F. *Solid State Ionics* **2002**, *147*, 181.
(40) Bouchet, R.; Siebert, E. *Solid State Ionics* **1999**, *118*, 287.
(41) Herz, H. G.; Kreuer, K. D.; Maier, J.; Scharfenberger, G.; Schuster, M. F. H.; Meyer, W. H. *Electrochim. Acta* **2003**, *48*, 2165.
(42) Noda, A.; Susan, Md. A. B. H.; Kudo, K.; Mitsushima, S.; Hayamizu, K.; Watanabe, M. *J. Phys. Chem. B* **2003**, *107*, 4024.
(43) Yamada, M.; Honma, I. *Chem. Phys. Lett.* **2005**, *402*, 324.
(44) Narayanan, S. R.; Yen, S.-P.; Liu, L.; Greenbaum, S. G. *J. Phys. Chem. B* **2006**, *110*, 3942.
(45) Yamada, M.; Honma, I. *J. Phys. Chem. B* **2004**, *108*, 5522.
(46) Qiao, J.; Hamaya, T.; Okada, T. *J. Mater. Chem.* **2005**, *15*, 4414.
(47) Chen, W. F.; Kuo, P. L. *Macromolecules* **2007**, *40*, 1987.
(48) Wang, T.; Gunasekaran, S. *J. Appl. Polym. Sci.* **2006**, *101*, 3227.
(49) Li, W.; Xue, F.; Cheng, R. *Polymer* **2005**, *46*, 12026.
(50) Baba, T.; Sakamoto, R.; Shibukawa, M.; Oguma, K. *J. Chromatogr. A* **2004**, *1040*, 45.
(51) Kim, Y. S.; Dong, L.; Hickner, M. A.; Glass, T. E.; Webb, V.; McGrath, J. E. *Macromolecules* **2003**, *36*, 6281.
(52) Liu, T. Y.; Chen, S. Y.; Lin, Y. L.; Liu, D. M. *Langmuir* **2006**, *22*, 9740.
(53) Tripathi, B. P.; Saxena, A.; Shahi, V. K. *J. Membr. Sci.* **2008**, *318*, 288.
(54) Miyatake, K.; Chikashige, Y.; Higuchi, E.; Watanabe, M. *J. Am. Chem. Soc.* **2007**, *129*, 3879.
(55) Lakshiminarayaiah, N. *Transport Phenomena in Membranes*; Academic Press: New York, 1969.
(56) Fischer, R. F. *Ind. Eng. Chem.* **1963**, *56*, 41.
(57) Bellami, L. J. *The Infrared Spectrum of Complex Molecules*, 2nd ed.; Wiley: New York, 1958.
(58) Socrates, G. *Infrared Characteristic Group Frequencies*; Wiley: New York, 1980.
(59) Vargas, M. A.; Vargas, R. A.; Mellander, B. E. *Electrochim. Acta* **2000**, *45*, 1399.
(60) Asano, N.; Akoi, M.; Suzuki, S.; Miyatake, K.; Uchida, H.; Watanabe, M. *J. Am. Chem. Soc.* **2006**, *128*, 1762.
(61) Yamaguchi, T.; Zhou, H.; Nakazawa, S.; Hara, N. *Adv. Mater.* **2007**, *19*, 592.
(62) Siu, A.; Schmeisser, J.; Holdcraft, S. *J. Phys. Chem. B* **2006**, *110*, 6072.
(63) Schaffer, T.; Tschinder, T.; Hacker, V.; Besenhard, J. O. *J. Power Sources* **2006**, *153*, 210.
(64) Zawodzinski, T. A.; Spinger, T. E.; Davey, J.; Jestal, R.; Lopez, C.; Valerino, J.; Gottesfeld, S. *J. Electrochem. Soc.* **1993**, *140*, 7.
(65) Zawodzinski, T. A.; Davey, J.; Valerino, J.; Gottesfeld, S. *Electrochim. Acta* **1995**, *40*, 297.

AM800228S